

1                   **An Ensemble-based Explicit Four-Dimensional Variational**  
2                                           **Assimilation Method**

3  
4  
5                   Xiangjun Tian<sup>1§</sup>, Zhenghui Xie<sup>1</sup> and Aiguo Dai<sup>2</sup>  
6

7  
8  
9                   1 Institute of Atmospheric Physics, Chinese Academy of Sciences, Beijing, China  
10                   (emails: [tianxj@mail.iap.ac.cn](mailto:tianxj@mail.iap.ac.cn); [zxie@lasg.iap.ac.cn](mailto:zxie@lasg.iap.ac.cn) )  
11

12                   2 National Center for Atmospheric Research, Boulder, Colorado, USA  
13                   (email: [adai@ucar.edu](mailto:adai@ucar.edu) )  
14

15  
16  
17  
18                   Submitted to *J. Geophys. Res.-Atmospheres*  
19                   Date: May 4, 2008  
20  
21

22  
23  
24  
25  
26  
27  
28  
29  
30  
31  
32  
33  
34  
35  
36  
37  
38  
39  
40  
41  
42

---

<sup>§</sup> *Corresponding author address:* X. Tian, Institute of Atmospheric Physics, Chinese Academy of Sciences, Beijing 100029, China; e-mail: [tianxj@mail.iap.ac.cn](mailto:tianxj@mail.iap.ac.cn)

43 ABSTRACT

44  
45 The adjoint and linearity models in the traditional four dimensional variational data  
46 assimilation (4DVAR) are difficult to obtain if the forecast model is highly nonlinear or the  
47 model physics contains parameterized discontinuities. A new method (referred to as POD-  
48 E4DVAR) is proposed in this paper by merging the Monte Carlo method and the proper  
49 orthogonal decomposition (POD) technique into the 4DVAR in order to transform an implicit  
50 optimization problem into an explicit one. The POD method is used to efficiently approximate a  
51 forecast ensemble produced by the Monte Carlo method in a 4-dimensional (4-D) space using a  
52 set of base vectors that span the ensemble and capture its spatial structure and temporal evolution.  
53 After the analysis variables being represented by a truncated expansion of the base vectors in the  
54 4-D space, the control (state) variables in the cost function appear explicitly, so that the adjoint  
55 model, which is used to derive the gradient of the cost function with respect to the control  
56 variables in the traditional 4DVAR, is no longer needed. The application of this new technique  
57 significantly simplifies the data assimilation process and retains the two main advantages of the  
58 traditional 4DVAR method. Assimilation experiments show that this ensemble-based explicit  
59 4DVAR method performs much better than the traditional 4DVAR and ensemble Kalman filter  
60 (EnKF) method. It is also superior to another explicit 4DVAR method, especially when the  
61 forecast model is imperfect and the forecast error comes from both the noise of the initial field  
62 and the uncertainty in the forecast model. Computational costs for the new POD-E4DVAR are  
63 about twice as the traditional 4DVAR method, but 5% less than the other explicit 4DVAR and  
64 much lower than the EnKF method.

65 **1. Introduction**

66 The four dimensional variational data assimilation (4DVAR) method [*Johnson et al.*,  
67 2006; *Kalnay et al.*, 2007; *Tsuyuki and Miyoshi*, 2007] has been a very successful technique used  
68 in operational numerical weather prediction (NWP) at many weather forecast centers [*Bormann*  
69 *and Thepaut*, 2004; *Park and Zou*, 2004; *Caya et al.*, 2005; *Bauer et al.*, 2006; *Rosmond and Xu*,  
70 2006; *Gauthier*, 2007]. The 4DVAR technique has two attractive features: 1) the physical model  
71 provides a strong dynamical constraint, and 2) it has the ability to assimilate the observational  
72 data at multiple times. However, 4DVAR still faces numerous challenges in coding, maintaining  
73 and updating the adjoint model of the forecast model and it requires the linearization of the  
74 forecast model. Usually, the control variables (or initial states) are expressed implicitly in the  
75 cost function. In order to compute the gradient of the cost function with respect to the control  
76 variables, one has to integrate the adjoint model, whose development and maintenance require  
77 significant resources, especially when the forecast model is highly nonlinear and the model  
78 physics contains parameterized discontinuities [*Xu*, 1996; *Mu and Wang*, 2003]. Many efforts  
79 have been devoted to avoid integrating the adjoint model or reduce the expensive computation  
80 costs [*Courtier et al.*, 1994; *Kalnay et al.*, 2000; *Wang and Zhao*, 2005], Nevertheless, the  
81 linearity of the forecast model is still required in all these methods. On the other hand, the usual  
82 ensemble Kalman Filter (EnKF) [e.g., *Evensen*, 1994, 2003; *Kalnay et al.*, 2007; *Beezley and*  
83 *Mandel*, 2008; also see Appendix A] has become an increasingly popular method because of its  
84 simple conceptual formulation and relative ease of implementation. For example, it requires no  
85 derivation of a tangent linear operator or adjoint equations, and no integrations backward in time.  
86 Furthermore, the computational costs are affordable and comparable with other popular and  
87 sophisticated assimilation methods such as the 4DVAR method. By forecasting the statistical

88 characteristics, the EnKF can provide flow-dependent error estimates of the background errors  
89 using the Monte Carlo method, but it lacks the dynamic constraint as in the 4DVAR. *Heemink*  
90 [2001] developed a variance reduced EnKF method by using a reduced-rank approximation  
91 technique to reduce the huge amount of computer costs. *Farrell and Ioannou* [2001] also  
92 proposed a reduced-order Kalman filter by the balanced truncation model-reduction technique.  
93 *Uzunoglu et al.* [2007] modified a maximum likelihood ensemble filter method [*Zupanski*, 2005]  
94 through an adaptive methodology. Generally, these three methods mentioned above belong to the  
95 Kalman filters. *Vermeulen and Heemink* [2006] have attempted to combine 4DVAR with the  
96 EnKF; however, the linearity model is still needed in their method. How to retain the two  
97 primary advantages of the traditional 4DVAR while avoiding the need of an adjoint or linearity  
98 model of the forecast model has become a roadblock in advancing data assimilation. Recently,  
99 *Qiu et al.* [*Qiu and Chou*, 2006; *Qiu et al.*, 2007a,b] proposed a new method for 4DVAR (more  
100 details below) using the singular value decomposition (SVD) technique based on the theory of  
101 the atmospheric attractors. *Cao et al.* [2006] has applied the proper orthogonal decomposition  
102 (POD) technique [*Ly and Tran*, 2001, 2002; *Volkwein*, 2008] to 4DVAR to reduce the forecast  
103 model orders while reducing the computational costs, but the adjoint integration is still necessary  
104 in their method.

105         Here we resort to the idea of the Monte Carlo method and the POD technique. The basic  
106 idea of the POD technique is to start with an ensemble of data, called *snapshots*, collected from  
107 an experiment or a numerical procedure of a physical system. The POD technique is then used to  
108 produce a set of base vectors which span the snapshot collection. The goal is to represent the  
109 ensemble of the data in terms of an *optimal* coordinate system. That is, the snapshots can be  
110 generated by a smallest possible set of base vectors. Based on this approach, an explicit new

111 4DVAR method is proposed in this paper: it begins with a 4-D ensemble obtained from the  
112 forecast ensembles at all times in an assimilation time window produced using the Monte Carlo  
113 method. We then apply the POD technique to the 4-D forecast ensemble, so that the orthogonal  
114 base vectors can not only capture the spatial structure of the state but also reflect its temporal  
115 evolution. After the model status being expressed by a truncated expansion of the base vectors  
116 obtained using the POD technique, the control variables in the cost function appear explicitly, so  
117 that the adjoint or linearity model is no longer needed.

118 Our new method was motivated by the need to merge the Monte Carlo method into the  
119 traditional 4DVAR in order to transform an implicit optimization problem into an explicit one.  
120 Our method not only simplifies the data assimilation procedure but also maintains the two main  
121 advantages of the traditional 4DVAR. This method is somewhat similar to Qiu et al.'s SVD-  
122 based method (referred to as SVD-E4DVAR hereafter, see Appendix B for details) because they  
123 both begin with a 4-D ensemble obtained from the forecast ensembles. However, they differ  
124 significantly in several aspects as discussed in section 2. *Hunter et al.* [2004], *John and Hunter*  
125 [2007] and *Szunyogh et al.* [2008] also developed a 4-D ensemble Kalman filter that infers the  
126 linearity model dynamics from the ensemble instead of the tangent-linear map as done in the  
127 traditional 4DVAR, in which the model states are expressed by the linear combinations of the  
128 ensemble samples directly rather than some orthogonal base vectors of the ensemble space. This  
129 method is also largely Kalman filtering, with the generation of its ensemble space being different  
130 from our method.

131 We conducted several numerical experiments using a one-dimensional (1-D) soil water  
132 equation and synthetical observations to evaluate our new method in land data assimilation.  
133 Comparisons were also made between our method, the SVD-E4DVAR [*Qiu and Chou*, 2006;

134 *Qiu et al.*, 2007a,b], traditional 4DVAR, and EnKF method. We found that our new ensemble-  
 135 based explicit 4DVAR (referred to as POD-E4DVAR) performs much better than the usual  
 136 EnKF method in terms of both increasing the assimilation precision and reducing the  
 137 computational costs. It is also better than the traditional 4DVAR and the SVD-E4DVAR,  
 138 especially when the forecast model is not perfect and the forecast error comes from both the  
 139 noise of the initial field and the uncertainty in the forecast model.

## 140 2. Methodology

141 In principle, the traditional, implicit 4DVAR (referred to as I4DVAR) analysis of  $\bar{x}_a$  is  
 142 obtained through the minimization of a cost function  $J$  that measures the misfit between the  
 143 model trajectory  $H_k(\bar{x}_k)$  and the observation  $\bar{y}_k$  at a series of times  $t_k, t = 1, 2, \dots, m$ :

$$144 \quad J(\bar{x}_0) = (\bar{x}_0 - \bar{x}_b)^T B^{-1} (\bar{x}_0 - \bar{x}_b) + \sum_{i=0}^m [\bar{y}_i - H_i(\bar{x}_i)]^T R_i^{-1} [\bar{y}_i - H_i(\bar{x}_i)], \quad (1)$$

145 with the forecast model  $M_{0 \rightarrow k}$  imposed as strong constraints, defined by

$$146 \quad \bar{x}_k = M_{0 \rightarrow k}(\bar{x}_0), \quad (2)$$

147 where the superscript  $T$  stands for a transpose,  $b$  is a background value, index  $k$  denotes the  
 148 observational time,  $H_k$  is the observational operator, and matrices  $B$  and  $R$  are the background  
 149 and observational error covariances, respectively. The control variable is the initial conditions  $\bar{x}_0$   
 150 (at the start of the assimilation time window) of the model. In the cost function (1) the control  
 151 variable  $\bar{x}_0$  is connected with  $\bar{x}_k$  through forwarding the model (2) and expressed implicitly,  
 152 which makes it difficult to compute the gradient of the cost function with respect to  $\bar{x}_0$ .

153 Assuming there are  $S$  time steps within the assimilation time window  $(0, T)$ . Generate  $N$   
 154 random perturbation fields using the Monte-Carol method and add each perturbation field to the

155 initial background field at  $t = t_0$  to produce  $N$  initial fields  $\bar{x}_n(t_0), n = 1, 2, \dots, N$ . Integrate the  
 156 forecast model  $\bar{x}_n(t_i) = M_i(\bar{x}_n(t_{i-1}))$  with the initial fields  $\bar{x}_n(t_0)(n = 1, 2, \dots, N)$  throughout the  
 157 assimilation time window to obtain the state series  $\bar{x}_n(t_i)(i = 0, 1, \dots, S - 1)$  and then construct the  
 158 perturbed 4-D fields (*snapshots*)  $\bar{X}_n(n = 1, 2, \dots, N)$  over the assimilation time window:

$$159 \quad \bar{X}_n = (\bar{x}_n(t_0), \bar{x}_n(t_1), \dots, \bar{x}_n(t_{S-1})), n = 1, 2, \dots, N. \quad (3)$$

160 It is obvious that such vectors can capture the spatial structure of the model state and its temporal  
 161 evolution. All the perturbed 4-D fields  $\bar{X}_n(n = 1, 2, \dots, N)$  can expand a finite dimensional space

162  $\Omega(\overbrace{\bar{X}_1 \bar{X}_2 \dots \bar{X}_N})$ . Similarly, the analysis field  $\bar{x}_a(t_i)(i = 0, 1, 2, \dots, S - 1)$  over the same assimilation  
 163 time window can also be stored into the following vector:

$$164 \quad \bar{X}_a = (\bar{x}_a(t_0), \bar{x}_a(t_1), \dots, \bar{x}_a(t_{S-1})). \quad (4)$$

165 When the ensemble size  $N$  is increased by adding random samples, the ensemble space could  
 166 cover the analysis vector  $\bar{X}_a$ , i.e.  $\bar{X}_a$  is approximately assumed to be embedded in the linear

167 space  $\Omega(\overbrace{\bar{X}_1 \bar{X}_2 \dots \bar{X}_N})$ . Let  $\bar{X}_{bn}(n = 1, 2, \dots, K, K \leq N)$  be the base vectors of this linear space

168  $\Omega(\overbrace{\bar{X}_1 \bar{X}_2 \dots \bar{X}_N})$ , the analysis vector  $\bar{X}_a$  can be expressed by the linear combinations of this set  
 169 of base vectors since it is in this space, i.e.

$$170 \quad \bar{X}_a = \sum_{n=1}^K \beta_n \bar{X}_{bn}, \quad (5)$$

171 Substituting (4) and (5) into (1), the control variable becomes  $\beta = (\beta_1 \dots \beta_K)^T$  instead of  $\bar{x}(t_0)$ ,  
 172 so the control variable is expressed explicitly in the cost function and the computation of the  
 173 gradient is simplified greatly. The linearity or adjoint model is no longer required. To minimize

174 the cost function, Eq. (1) is transformed into an explicit optimization problem with the variable  
 175 vector  $\beta = (\beta_1 \cdots \beta_k)^T$ , which can be solved by the usual optimization algorithms, such as the  
 176 quasi-Newton method. It is noted that, unlike EnKF, only one analyzed field is obtain in each  
 177 analysis procedure in the POD-E4DVAR and the initial condition should be perturbed at the start  
 178 time of the assimilation in each cycle.

179 How to obtain the appropriate base vectors remains the only task left. We found that the  
 180 POD technique is a good choice for doing this. It can produce a set of base vectors spanning the  
 181 ensemble of data in certain least squares optimal sense (see Appendix C).

182 The average of the ensemble of snapshots is given by

$$183 \quad \bar{X} = \frac{1}{N} \sum_{n=1}^N \bar{X}_n, \quad (6)$$

184 We form a new ensemble by focusing on deviations from the mean as follows

$$185 \quad \delta X_n = \bar{X}_n - \bar{X}, n = 1, \cdots N, \quad (7)$$

186 which form the matrix  $A (M \times N)$ , where  $M = M_g \times M_v \times S$ , and  $M_g, M_v$  are the number of the  
 187 model spatial grid points and the number of the model variables respectively. To compute the  
 188 POD modes, one must solve an  $M \times M$  eigenvalue problem:

$$189 \quad (AA^T)_{M \times M} V = \lambda V$$

190 In practice, the direct solution of this eigenvalue problem is often not feasible if  $M \gg N$ , which  
 191 occurs often in numerical models. We can transform it into an  $N \times N$  eigenvalue problem  
 192 through the following transformations:

$$193 \quad ((AA^T)_{M \times M} V)^T = (\lambda V)^T,$$

$$194 \quad V^T A^T A = V^T \lambda^T,$$

195 
$$A^T AV = \lambda^T V .$$

196 In the method of snapshots, one then solves the  $N \times N$  eigenvalue problem

197 
$$TV_k = \lambda_k V_k, k = 1, \dots, N , \quad (8)$$

198 where  $T = (A^T A)_{N \times N}$ ,  $V_k$  is the  $k$ th column vector of  $V$  and  $\lambda_k$  is the  $k$ th row vector of  $\lambda$  .

199 The nonzero eigenvectors  $\lambda_k$  ( $1 \leq k \leq N$ ) may be chosen to be orthonormal, and the POD modes  
 200 are given by  $\phi_k = AV_k / \sqrt{\lambda_k}$ , ( $1 \leq k \leq N$ ).

201 The truncated reconstruction of analysis variable in the four dimensional space  $\bar{X}_a$  is given  
 202 by

203 
$$\bar{X}_a = \bar{X} + \sum_{j=1}^P \alpha_j \phi_j , \quad (9)$$

204 where  $P$  (the number of the POD modes) is defined as follows

205 
$$P = \min \left\{ P, I(P) = \frac{\sum_{i=1}^P \lambda_i}{\sum_{i=1}^N \lambda_i} : I(P) \geq \gamma \right\}, 0 < \gamma \leq 1. \quad (10)$$

206 It is well known [Ly and Tran, 2001, 2002] that the expansion (9) is optimal. In particular,  
 207 among all linear combinations (including the linear combinations based on the SVD base  
 208 vectors), the POD is the most efficient, in the sense that, for a given number of modes  $P$ , the  
 209 POD decomposition captures the most possible kinetic energy. The solution for the analysis  
 210 problem is approximately expressed by a truncated expansion of the POD base vectors in the 4-D  
 211 space. Substituting (9) and (4) into (1), the control variable becomes  $\alpha = (\alpha_1, \alpha_2, \dots, \alpha_p)^T$  instead  
 212 of  $\bar{x}_0$ , so the control variable is expressed explicitly in the cost function and the linearity or  
 213 adjoint model is not needed any more.

214           The two explicit methods (the SVD- and POD-based methods) share some similar  
215 features: for example, they both begin with a 4-D ensemble and do not need the linearity or  
216 adjoint model. However, the POD-E4DVAR method differs from the SVD-E4DVAR  
217 significantly in three aspects: 1) the 4-D sample in the SVD-E4DVAR method is only composed  
218 of the state vectors at the observational times over the assimilation time window, while it is  
219 composed of the state vectors at all the time steps over the assimilation time window in the POD-  
220 E4DVAR method. The latter contains the most possible forecast information in the assimilation  
221 time window. 2) The SVD technique is used to generate the set of base vectors in the SVD-  
222 E4DVAR, while the POD-E4DVAR adopts the POD method, which captures the most possible  
223 kinetic energy of the ensemble space because of its optimality. And 3) The application of matrix  
224 transformation technique in the POD-E4DVAR greatly lowers the computational costs by  
225 reducing the decomposition into an  $N \times N$  eigenvalue problem ( $N \ll M$ ).

### 226 **3. Numerical experiments**

227           In this section, the applicability of this new method is evaluated through several  
228 assimilation experiments with a simple 1-D soil water equation model used in the NCAR  
229 Community Land Model (CLM) [Oleson *et al.*, 2004]. In addition, we also compare assimilation  
230 results using the SVD-E4DVAR, I4DVAR, and EnKF methods.

#### 231 **3.1. Set-up of experiments**

232           The volumetric soil moisture ( $\theta$ ) for 1-D vertical water flow in a soil column in the CLM  
233 is expressed as

$$234 \quad \frac{\partial \theta}{\partial t} = -\frac{\partial q}{\partial z} - E - R_{fm} , \quad (11)$$

235 where  $q$  is the vertical soil water flux ,  $E$  is the evapotranspiration rate, and  $R_{fm}$  is the melting  
 236 (negative) or freezing (positive) rate, (for simplicity,  $E, R_{fm}$  are taken as zero in the experiments),  
 237 and  $z$  is the depth from the soil surface. Both  $q$  and  $z$  are positive downward.

238 The soil water flux  $q$  is described by Darcy's law [Darcy, 1856]:

$$239 \quad q = -k \frac{\partial(\varphi + z)}{\partial z}, \quad (12)$$

240 where  $k = k_s \left( \frac{\theta}{\theta_s} \right)^{2b+3}$  is the hydraulic conductivity, and  $\varphi = \varphi_s \left( \frac{\theta}{\theta_s} \right)^{-b}$  is the soil matrix  
 241 potential ,  $k_s, \varphi_s, \theta_s$  and  $b$  are constants. The CLM computes soil water content in the 10 soil  
 242 layers through (11-12) (see [Oleson *et al.*, 2004] for details). The upper boundary condition is

$$243 \quad q_0(t) = -k \frac{\partial(\varphi + z)}{\partial z} \Big|_{z=0}, \quad (12b)$$

244 where  $q_0(t)$  is the water flux at the land surface (referred to as infiltration), and the lower  
 245 boundary condition is  $q_l = 0$ . The time step  $\Delta t$  is 1800 s (0.5 hour).

246 We took a site at (47.43°N, 126.97°E) as the experimental site. The soil parameters  
 247  $k_s, \varphi_s, \theta_s$  and  $b$  at this site were calculated by the CLM using the high-resolution soil texture  
 248 data released with the CLM by NCAR:  $\theta_s = 0.46 \text{m}^3/\text{m}^3$ ,  $k_s = 2.07263\text{E-}6$  m/s,  $b = 8.634$ ,  $\varphi_s =$   
 249  $3.6779\text{m}$ . We then ran the model at the site forced with observation-based 3-hourly forcing data  
 250 [Qian *et al.*, 2005; Tian *et al.*, 2007] from January 1, 1992 to December 31, 1993 after ten-year  
 251 spinning-up to obtain a two-year time series of simulated infiltration (i.e., the water flux  $q$  at the  
 252 surface, c.f., Eq.(12b)) for driving the soil water hydrodynamic equation (11). We used the first  
 253 year (January 1, 1992 to December 31, 1992) data of CLM-simulated infiltration as the “perfect”  
 254 infiltration series, and took the second year data as the “imperfect” infiltration series (Fig. 1). In

255 our experiments, we integrated the soil water hydrodynamic equation (11) forced by the two  
 256 infiltration time series for 365 days separately: Eq. (11) forced by the “perfect” infiltration series  
 257 represents the perfect *forecast model*, whose forecast error comes only from the noise in the  
 258 initial (soil moisture) field; on the contrary, Eq. (11) forced by the “imperfect” infiltration series  
 259 acts as the “imperfect” forecast model, whose forecast error comes from not only the noise of the  
 260 initial field but also the uncertainty in the forecast model itself.

261 Figure 2 shows the “imperfect” and the “perfect” initial soil moisture profiles (which are  
 262 obtained by randomly taking two arbitrary CLM-simulated soil moisture profiles in the process  
 263 of the infiltration series producing), which denote the initial fields with and without noise. The  
 264 “perfect” (or “true”) state was produced by integrating the “perfect” model with the “perfect”  
 265 initial soil moisture profile for 365 days. The “observations” were generated by adding 3%  
 266 random error perturbation to the time series of the “perfect” state (i.e., “observation” =  
 267  $(1 + \varepsilon) \times \text{“perfect”}$ , where  $\varepsilon$  is a real random number varying from -3% to 3%), and these  
 268 “observations” were assimilated using the various methods in the assimilation experiments (but  
 269 not in the forecast experiments). In addition, two separate forecast states were produced by  
 270 integrating the perfect and imperfect models with the “imperfect” initial soil moisture separately:  
 271 for the former case, the forecast error comes only from the noise in the initial field, but in the  
 272 latter case it comes from both the noise and the uncertainty in the forecast model.

273 The length of an assimilation time window in our experiments is one day (48 time steps),  
 274 i.e.  $S = 48$  . The size of  $\bar{X}_n = (\bar{x}_n(t_1), \bar{x}_n(t_2), \dots, \bar{x}_n(t_{S-1}))$  in our method is 480,  
 275 where  $\bar{x}_n(t_i) = (\theta_{n1}(t_i), \theta_{n2}(t_i), \dots, \theta_{n10}(t_i))$  and  $M_g = 10, M_v = 1$ . The background and observational  
 276 error covariance matrices used in the E/I4DVAR methods can be obtained by using the ensemble

277 covariance matrices defined by Eqs. (a.4) and (a.8) in Appendix A, respectively. We  
 278 used  $\gamma = 0.90$  in our experiments.

279 Two groups of experiments were done: The perfect model with the “imperfect” initial field  
 280 as Group 1 and the imperfect model with the “imperfect” initial field as Group 2. Three  
 281 observation sampling frequencies (hourly, 2-hourly, and 3-hourly) were tested in each group’s  
 282 experiments. The ensemble size used in the POD- and SVD-E4DVAR and EnKF methods was  
 283 60 in this study (the impact of the ensemble size on the assimilation results will be discussed in  
 284 another study). The linearization of the soil moisture equation (11) follows the format in *Zhang*  
 285 *et al.* [2001].

### 286 3.2. Experimental results

287 To evaluate the performance of the four algorithms (POD/SVD-E4DVAR, I4DVAR and  
 288 EnKF), a relative error is defined as follows

$$289 \quad E_{t_{0 \rightarrow S-1}} = \frac{\sum_{i=0}^{S-1} \sum_{j=1}^{M_s \times M_v} (\bar{x}_j^a(t_i) - \bar{x}_j^t(t_i))^2}{\sum_{i=0}^{S-1} \sum_{j=1}^{M_s \times M_v} (\bar{x}_j^f(t_i) - \bar{x}_j^t(t_i))^2}, \quad (13)$$

290 where the index  $t_{0 \rightarrow S-1}$  denotes an assimilation time window (one day in our experiments),  $S$  is  
 291 the length of an assimilation window ( $S = 48$  in our experiments),  $f$  and  $a$  denote the forecast  
 292 state (without assimilation of the “observations”) and the analysis state, respectively,  $t$   
 293 represents the “true” (“perfect”) state. Thus, a relative error of 1% for a given assimilation  
 294 method would mean that the mean error of the analyzed soil moisture is only 1% of that in the  
 295 forecast case.

296 Figures 3-4 show that the POD/SVD-E4DVAR methods perform much better than the EnKF  
 297 and the I4DVAR methods in both groups of experiments. The two explicit 4DVAR methods

298 perform almost same in Group 1 experiments. Their relative errors for analyzed soil moisture are  
299 very small (less than 1%) in the case that the forecast model is perfect, in which the forecast  
300 error comes only from the noise of the initial field (Fig. 3). However, the relative errors of the  
301 EnKF method are many times higher than those of POD/SVD-E4DVAR, around 1~ 2% or so.  
302 The traditional 4DVAR method performs even worse than the EnKF, which is consistent with  
303 the results of *Reichle et al.* [*Reichle and Entekhabi, 2001; Reichle et al., 2002a,b*]. This is  
304 expected because the soil water hydrodynamic equation (11) is a highly nonlinear system and the  
305 tangent linearization operator used in the usual 4DVAR can only propagate analytically with the  
306 first-order precision, which introduces large errors in variable estimation and leads to sub-  
307 optimal performance.

308       When the forecast model is imperfect, its forecast error comes from both the noise of the  
309 initial field and the uncertainty in the model itself. The relative errors of the four methods all  
310 become larger in this case (Fig. 4), presumably due to the reduced effect of data assimilation  
311 under a poorly constrained model. Nevertheless, the relative errors for the POD-E4DAVR are  
312 substantially smaller than those of the other methods, including the SVD-E4DVAR which  
313 performs similarly with the EnKF in this case: most of the POD-E4DVAR relative errors are still  
314 controlled in the magnitude between 0 and 6 %, however many of the relative errors of I4DVAR  
315 (also the SVD-E4DVAR) method are higher than 6%, and some are even up to 10%; It is also a  
316 bit surprising that the SVD-based method is apparently inferior to the POD-E4DVAR in some  
317 assimilation time windows and even worse than the EnKF method (Fig. 4). Figs.3-4 also show  
318 that the observation frequency has larger impacts in the I4DVAR method than in the POD-  
319 E4DVAR method.

320 For the two groups of experiments, the ratio of the computational costs for the four methods  
321 (POD-E4DVAR: SVD-E4DVAR: I4DVAR : EnKF) is about 1 : 1.05 : 0.5 : 30. The high  
322 computational cost in EnKF method is mainly due to the fact the analysis process composed of  
323 huge matrix computations has to be conducted repeatedly at every time step in the assimilation  
324 time window, while that in POD-E4DVAR is performed only once in each cycle correspondingly.  
325 The 5% reduction in the POD-E4DVAR compared with the SVD-E4DVAR results from the  
326 application of the matrix transformation technique described in section 2. The main  
327 computational costs of the POD-E4DVAR come from the ensemble integrations over the  
328 assimilation time window, which can be done on parallel computers. Thus, the additional costs  
329 of the POD-E4DVAR compared with the traditional 4DVAR should not result in real difficulties,  
330 and it still costs only one thirtieth of that of the EnKF method in our experiments.

#### 331 **4. Summary and concluding remarks**

332 To retain the main strength of traditional 4DVAR while avoiding the need of an adjoint or  
333 linearity model of the forecast model in data assimilation, we have developed an ensemble-based  
334 explicit 4DVAR method in this paper (called POD-E4DVAR). This new method merges the  
335 Monte Carlo method and the proper orthogonal decomposition (POD) technique into the 4DVAR  
336 to transform an implicit optimization problem into an explicit one. The POD method efficiently  
337 approximates a forecast ensemble produced by the Monte Carlo method in a 4-D space using a  
338 set of base vectors that span this ensemble and capture its spatial structure and temporal  
339 evolution. After the analysis variables being represented by a truncated expansion of the base  
340 vectors in the 4-D space, the control (state) variables in the cost function appear explicitly, so  
341 that the adjoint model, which is used to derive the gradient of the cost function with respect to  
342 the control variables in traditional 4DVAR, is no longer needed. This new method significantly

343 simplifies the data assimilation process and retains the two main advantages of the traditional  
344 4DVAR (i.e., dynamic constraint and assimilation of observations).

345         Several numerical experiments performed with a simple 1-D soil water equation show that  
346 the new POD-E4DVAR method performs much better than the traditional 4DVAR and EnKF  
347 method with assimilation errors being reduced to a fraction of the latter two. It is also superior to  
348 the SVD-E4DVAR, another explicit 4DVAR method developed by *Qiu et al.* [2007a,b],  
349 especially when the forecast model is imperfect and the error comes from both the noise of the  
350 initial field and the uncertainty in the forecast model. In our experiments, the traditional (implicit)  
351 4DVAR method performs worst, which is due to errors associated with the tangent linearization  
352 operator used in the usual 4DVAR that only propagates analytically with the first-order precision.  
353 The results show that the POD-E4DVAR method provides a promising new tool for data  
354 assimilation.

355         Several issues, such as the impacts of the ensemble size and the initial perturbation fields  
356 on the assimilated results and the actual performance of this new method in real numerical  
357 forecast models, still need to be addressed. Another potential issue existing in our method should  
358 be specially mentioned: since this method begins with a 4-D ensemble obtained from the  
359 perturbed ensembles, the quality of the results relies on the perturbation method a lot. How to  
360 generate a reasonable perturbed field is a critical step in using this method, which also requires  
361 further investigation.

362 *Acknowledgments.* This work was supported by the National Natural Science Foundation of  
363 China under Grant No. 40705035, the Knowledge Innovation Project of Chinese Academy of  
364 Sciences under Grant No. KZCX2-YW-217 and NO. KZCX2-YW-126-2, and the National Basic

365 Research Program under the Grant 2005CB321704. The National Center for Atmospheric  
 366 Research is sponsored by the U.S. National Science Foundation.

367

## 368 **Appendix A: The Ensemble Kalman Filter (EnKF) Method**

### 369 **A.1 Ensemble representation for covariance matrix**

370 One can define the matrix holding the ensemble members  $\vec{x}_i \in R^n$  as

$$371 \quad A = (\vec{x}_1, \vec{x}_2, \dots, \vec{x}_N) \in R^{n \times N}, \quad (\text{a.1})$$

372 where  $N$  is the number of ensemble members and  $n$  is the size of the model state vector.

373 The ensemble mean is stored in each column of  $\bar{A}$  which can be defined as

$$374 \quad \bar{A} = A 1_N, \quad (\text{a.2})$$

375 where  $1_N \in R^{N \times N}$  is a matrix in which each element is equal to  $1/N$ . One can then define the  
 376 ensemble perturbation matrix as

$$377 \quad A' = A - \bar{A} = A(I - 1_N), \quad (\text{a.3})$$

378 The ensemble covariance matrix  $P_e \in R^{n \times n}$  can be defined as

$$379 \quad P_e = \frac{A'(A')^T}{N-1}. \quad (\text{a.4})$$

### 380 **A.2 Measurement perturbations**

381 Given a vector of measurements  $y \in R^m$ , with  $m$  being the number of measurements, one  
 382 can define  $N$  vectors of perturbed observations as

$$383 \quad \bar{y}_j = \bar{y} + \varepsilon_j, j = 1, 2, \dots, N, \quad (\text{a.5})$$

384 which can be stored in the columns of a matrix

$$385 \quad Y = (\bar{y}_1, \bar{y}_2, \dots, \bar{y}_N) \in R^{m \times N}, \quad (\text{a.6})$$

386 while the ensemble of perturbations, with ensemble mean equal to zero, can be stored in the  
 387 matrix

$$388 \quad E = (\varepsilon_1, \varepsilon_2, \dots, \varepsilon_N) \in R^{m \times N}, \quad (\text{a.7})$$

389 from which we can construct the ensemble representation of the measurement error covariance  
 390 matrix

$$391 \quad R_e = \frac{EE^T}{N-1}, \quad (\text{a.8})$$

### 392 **A.3 Analysis equation**

393 The analysis equation, expressed in terms of the ensemble covariance matrices, is

$$394 \quad A^a = A + P_e H^T (H P_e H^T + R_e)^{-1} (D - HA). \quad (\text{a.9})$$

395 Using the ensemble of innovation vectors defined as

$$396 \quad D' = D - HA, \quad (\text{a.10})$$

397 and the definitions of the ensemble error covariance matrices in Eqs.(a.4) and (a.8), the analysis  
 398 can be expressed as

$$399 \quad A^a = A + A' A'^T H^T (H A' A'^T H^T + EE^T)^{-1} D'. \quad (\text{a.11})$$

400 When the ensemble size,  $N$ , is increased by adding random samples, the analysis computed  
 401 from this equation will converge towards the exact solution of Eq.(a.9) with  $P_e$  and  $R_e$  replaced  
 402 by the exact covariance matrices  $P$  and  $R$ .

### 403 **Appendix B: The SVD-E4DVAR Method**

404 Assuming there are  $m$  observations  $\bar{y}_i (i = 0, 1, \dots, m-1)$  at time  $t = t_0, \dots, t_i, \dots, t_{m-1}$  during  
 405 the assimilation time window. Generate  $N$  random perturbation fields and add each to the initial  
 406 background field and integrate the model to produce a perturbed 4-D field over the analysis time  
 407 window. The  $i$ th difference field is then given by  $\delta \vec{x}_i = \vec{x}_i - \vec{x}_b$  at time  $t = t_0, \dots, t_i, \dots, t_{m-1}$ , where

408  $\bar{x}_b, \bar{x}_i$  denote the background and the perturbed fields, respectively. Consider an ensemble of  
 409 column vectors represented by matrix  $A = (\delta\bar{X}_1, \delta\bar{X}_2, \dots, \delta\bar{X}_N)$ , where the  $i$ th column vector  
 410  $\delta\bar{X}_i$  represents the  $i$ th sampled data field in a discrete four-dimensional analysis space. The  
 411 length of vector  $\delta\bar{X}_i$  is  $M_g \times M_v \times m$ , where  $M_g, M_v$  are the number of the model spatial grid  
 412 points and the number of the model variables, respectively. The SVD of  $A$  yields

$$413 \quad A = B\Lambda V^T, \quad (b.1)$$

414 where  $\Lambda$  is a diagonal matrix composed of the singular values of  $A$  with  $\lambda_1 \geq \lambda_2 \geq \dots \geq \lambda_r$  and  
 415  $\lambda_{r+1} = \lambda_{r+2} = \dots = 0$ ,  $r \leq \min(M_g \times M_v \times m, N)$ , is the rank of  $A$ ,  $B$  and  $V$  are orthogonal  
 416 matrices composed of the left and right singular vectors of  $A$ , respectively. The SVD in (b.1)  
 417 gives  $C = A^T A = V\Lambda^2 V^T$  and  $Q = AA^T = B\Lambda^2 B^T$ . Thus, the  $i$ th column vector of  $V$ , denoted by  
 418  $V_i$ , is the  $i$ th eigenvector of  $C$ , while the  $j$ th column vector of  $B$ , denoted by  $b_j$ , is the  $j$ th  
 419 column vector of  $Q$  and is called the singular vector of  $A$ .

420 The truncated reconstruction of analysis variable  $\bar{X}_a$  in 4-D space is given by

$$421 \quad \bar{X}_a = \bar{X}_b + \sum_{i=1}^P \alpha_i b_i, \quad (b.2)$$

422 where  $P(\leq r)$  is the truncation number, which can be obtained through Eq.(10) in section 2,

423  $\bar{X}_b = (\bar{x}_b, \bar{x}_b, \dots, \bar{x}_b)$  is composed of  $m$  vectors  $(\bar{x}_b)$ .

424 Substituting (b.2) into Eq. (1) in section 2, the control variable becomes  $\alpha$  instead of  $\bar{x}_0$ , so  
 425 the control variable is expressed explicitly in the cost function.

## 426 **Appendix C: The Proper Orthogonal Decomposition**

### 427 **Continuous case**

428 Let  $U_i(\vec{x}), i=1,2,\dots,N$  denote the set of  $N$  observations or simulations (also called  
 429 *snapshots*) of some physical process taken at position  $\vec{x}=(x,y)$ . The average of the ensemble  
 430 snapshots is given by

$$431 \quad \bar{U} = \frac{1}{N} \sum_{i=1}^N U_i(\vec{x}), \quad (c.1)$$

432 We form new ensemble by focusing on deviation from mean as follows:

$$433 \quad V_i = U_i - \bar{U}, \quad (c.2)$$

434 We wish to find an optimal compressed description of the sequence of data (c.2). One  
 435 description of the process is a series expansion in terms of a set of base functions. Intuitively, the  
 436 base functions should in some sense be representative of the members of the ensemble. Such a  
 437 coordinate system, is provided by the Karhunan Loève expansion, where the base functions  $\Phi$   
 438 are, in fact, admixtures of the snapshots and are given by:

$$439 \quad \Phi = \sum_{i=1}^N a_i V_i(\vec{x}), \quad (c.3)$$

440 Here, the coefficients  $a_i$  are to be determined so that  $\Phi$  given by (c.3) will resemble the

441 ensemble  $\{V_i(\vec{x})\}_{i=1}^N$  most closely. More specifically, we look for a function  $\Phi$  to maximize

$$442 \quad \frac{1}{N} \sum_{i=1}^N |(V_i, \Phi)|^2, \quad (c.4)$$

443 subjected to  $(\Phi, \Phi) = \|\Phi\|^2 = 1$ , where  $(\cdot, \cdot)$  and  $\|\cdot\|$  denote the usual  $L^2$  inner product and  $L^2$ -  
 444 norm, respectively.

445 It follows that the base functions are the eigenfunctions of the integral equation

$$446 \quad \int C(\vec{x}, \vec{x}') \Phi(\vec{x}') d\vec{x}' = \lambda \Phi(\vec{x}), \quad (c.5)$$

447 Substituting (c.3) into (c.5) yields the eigenvalue problem:

448 
$$\sum_{j=1}^N L_{ij} a_j = \lambda a_i, \quad (\text{c.6})$$

449 where  $L_{ij} = \frac{1}{N} (V_i, V_j)$  is a symmetric and nonnegative matrix. Thus, our problem amounts to

450 solving for the eigenvectors of an  $N \times N$  matrix, where  $N$  is the ensemble size of the snapshots.

451 Straightforward calculation shows that the cost function

452 
$$\frac{1}{N} \sum_{i=1}^N |(V_i, \Phi)|^2 = (\lambda \Phi, \Phi) = \lambda, \quad (\text{c.7})$$

453 is maximized when the coefficients  $a_i$ 's of (c.3) are the elements of the eigenvector

454 corresponding to the largest eigenvalue of  $L$ .

455 **Discrete case**

456 We consider the discrete Karhunan Loève expansion to find an optimal representation of

457 the ensemble of snapshots. In the two-dimensional case, each sample of snapshots  $U_i(x, y)$

458 (defined on a set of  $n \times n$  nodal points  $(x, y)$ ) can be expressed as an  $n^2$  dimensional vector  $\vec{u}_i$

459 as follows:

460 
$$\vec{u}_i = \begin{bmatrix} \vec{u}_{i1} \\ \vdots \\ \vec{u}_{ij} \\ \vdots \\ \vec{u}_{in^2} \end{bmatrix}, \quad (\text{c.8})$$

461 where  $\vec{u}_{ij}$  denotes the  $j$ th component of the vector  $\vec{u}_i$ . Here the discrete covariance matrix of the

462 ensemble  $\vec{u}$  is defined as

463 
$$C_u = E \left\{ (\vec{u} - \vec{m}_u)(\vec{u} - \vec{m}_u)^T \right\}, \quad (\text{c.9})$$

464 where

$$465 \quad \vec{m}_u = E\{\vec{u}\} \quad (c.10)$$

466 is the mean vector,  $E$  is the expected value. Eqs. (c.9) and (c.10) can be replaced by

$$467 \quad C_u = \frac{1}{N} \left[ \sum_{i=1}^N \vec{u}_i \vec{u}_i^T \right] - \vec{m}_u \vec{m}_u^T$$

468 and

$$469 \quad \vec{m}_u = \frac{1}{N} \sum_{i=1}^N \vec{u}_i$$

470 respectively.

471

472

#### 473 REFERENCES

- 474 Bauer, P., P. Lopez, A. Benedetti, D. Salmond, S. Saarinen, and M. Bonazzola (2006),  
475 Implementation of 1D+4D-Var assimilation of precipitation-affected microwave radiances  
476 at ECMWF. II: 4D-Var, *Q. J. Roy. Meteorol. Soc.*, *132*, 2307–2332.
- 477 Beezley, J. D., and J. Mandel (2008), Morphing ensemble Kalman filters, *Tellus A*, *60(1)*, 131-  
478 140.
- 479 Bormann, N., and J. N. Thepaut (2004), Impact of MODIS polar winds in ECMWF's 4DVAR  
480 data assimilation system, *Mon. Wea. Rev.*, *132*, 929-940.
- 481 Cao, Y., J. Zhu, I. M. Navon, and Z. D. Luo (2007), A reduced order approach to four-  
482 dimensional variational data assimilation using proper orthogonal decomposition, *Intl. J.*  
483 *Num. Methods Fluids*, *53*, 1571–1583, doi: 10.1002/flid.1365.
- 484 Caya, A., J. Sun, and C. Snyder (2005), A comparison between the 4DVAR and the ensemble  
485 Kalman filter techniques for radar data assimilation, *Mon. Wea. Rev.*, *133*, 3081-3094.

486 Courtier, P., J. N. Thepaut, and A. Hollingsworth (1994), A strategy for operational  
487 implementation of 4DVAR, using an incremental approach, *Q. J. R. Meteorol Soc.*, 120,  
488 1367–1387.

489 Darcy, H. (1856), *Les Fontaines Publiques de la Ville de Dijon*, Dalmont, Paris.

490 Evensen, G. (1994), Sequential data assimilation with a non-linear geostrophic model using  
491 Monte Carlo methods to forecast error statistics, *J. Geophys. Res.*, 99(C5), 10143-10162.

492 Evensen, G. (2003), The Ensemble Kalman Filter: theoretical formulation and practical  
493 implementation, *Ocean Dynamics*, 53, 343–367

494 Farrell, B. F., and P. J. Ioannou (2001), State estimation using a reduced order Kalman filter, *J.*  
495 *Atmos. Sci.*, 58, 3666-3680.

496 Gauthier, P., M. Tanguay, S. Laroche, S. Pellerin, and J. Morneau (2007), Extension of 3DVAR  
497 to 4DVAR: Implementation of 4DVAR at the Meteorological Service of Canada, *Mon. Wea.*  
498 *Rev.*, 135(6), 2339-2354.

499 Heemink, A.W., M. Verlaan, and A. J. Segers (2001), Variance reduced ensemble Kalman  
500 filtering, *Mon. Wea. Rev.*, 129(7), 1718-1728.

501 Hunt B. R., E. Kalnay, E. J. Kostelich, and E. Ott, et al. (2004), Four-dimensional ensemble  
502 Kalman filtering, *Tellus A*, 56, 273-277.

503 Ly, H. V., and H.T. Tran (2001), Modeling and control of physical processes using proper  
504 orthogonal decomposition, *Mathematical and Computer Modeling*, 33, 223-236.

505 Ly, H. V., and H.T. Tran (2002), Proper orthogonal decomposition for flow calculations and  
506 optimal control in a horizontal CVD reactor, *Quarterly of Applied Mathematics*, 60(3), 631-  
507 656.

508 John, H., and B. R. Hunt (2007), Four-dimensional local ensemble transform Kalman filter:

509 numerical experiments with a global circulation model, *Tellus A*, 59, 731-748.

510 Johnson, C., B. J. Hoskins, N. K. Nichols, and S. P. Ballard (2006), A singular vector perspective  
511 of 4DVAR: The spatial structure and evolution of baroclinic weather systems, *Mon. Wea.*  
512 *Rev.*,134(11), 3436-3455.

513 Kalnay, E., H. Li, T. Miyoshi, S. C. Yang, and J. Ballabrera-Poy (2007), 4-D-Var or ensemble  
514 Kalman filter?, *Tellus A*, 59(5), 758-773.

515 Kalnay E., S. K. Park, and Z. X. Pu et al. (2000), Application of the quasi-inverse method to data  
516 assimilation, *Mon. Wea. Rev.*, 128,864-875.

517 Mu, M., J. Wang (2003), A method for adjoint variational data assimilation with physical “on-  
518 off” processes, *J Atmos Sci*, 60, 2010-2018.

519 Oleson, K. W., Y. Dai, G. Bonan, M. Bosilovich, R. Dickinson, P. Dirmeyer, F. Hoffman, P.  
520 Houser, S. Levis, G.-Y. Niu, P. Thornton, M. Vertenstein, Z.-L. Yang, and X. Zeng (2004),  
521 *Technical description of the community land model (CLM)*, NCAR/TN-461+STR, 186pp.

522 Park, K., and X. Zou (2004), Toward developing an objective 4DVAR BDA scheme for  
523 hurricane initialization based on TPC observed parameters, *Mon. Wea. Rev.*,132(8),2054-  
524 2069.

525 Qian, T., A. Dai, K. E. Trenberth and Keith W. Oleson (2006), Simulation of global land surface  
526 conditions from 1948 to 2004. Part I: Forcing data and evaluations, *J. Hydrometeor.*, 7, 953-  
527 975.

528 Qiu, C. J., and J. F. Chou (2006), Four-dimensional data assimilation method based on SVD:  
529 theoretical aspect, *Theor Appl Climatol*, 83, 51-57.

530 Qiu, C. J., L. Zhang and A. M. Shao(2007a), An explicit four-dimensional variational data  
531 assimilation method, *Science in China (D)*, 50(8), 1232-1240.

532 Qiu, C. J., A. M. Shao, Q. Xu, and L. Wei (2007b), Fitting model fields to observations by using  
533 singular value decomposition: An ensemble-based 4DVar approach, *J. Geophys. Res.*,  
534 *112*, D11105, doi:10.1029/2006JD007994

535 Reichle, R. H., and D. Entekhabi (2001), Downscaling of radio brightness measurements for soil  
536 moisture estimation: A four-dimensional variational data assimilation approach, *Water*  
537 *Resour. Res.*, *37* (9), 2 353-2 364.

538 Reichle, R. H., J. P. Walker, and R. D. Koster et al. (2002a), Extended versus ensemble filtering  
539 for land data assimilation, *Journal of hydrometeorology*, *3*, 728-740.

540 Reichle, R. H., D. B. McLaughlin, and D. Entekhabi (2002b), Hydrologic data assimilation with  
541 the ensemble Kalman filter, *Mon. Wea. Rev.*, *130*, 103-114.

542 Rosmond, T., and L. Xu (2006), Development of NAVDAS-AR: non-linear formulation and  
543 outer loop tests. *Tellus A*, *58*(1), 45-58.

544 Szunyogh, I., E. J. Kostelich, G. Gyarmati, E. Kalnay, B. R. Hunt, E. Ott, E. Satterfield, and J. A.  
545 Yorke (2008), A local ensemble transform Kalman filter data assimilation system for the  
546 NCEP global model, *Tellus A*, *60*(1), 113-130.

547 Tian, X., A. Dai, D. Yang and Z. Xie (2007), Effects of precipitation-bias corrections on surface  
548 hydrology over northern latitudes, *J. Geophys. Res.*, *112*, D14101, doi:10.  
549 029/2007JD008420.

550 Tsuyuki, T., and T. Miyoshi (2007). Recent progress of data assimilation methods in  
551 meteorology, *Journal of the Meteorological Society of Japan*, *85B*, 331-361.

552 Vermeulen, P. T. M., and A. W. Heemink (2006), Model-reduced variational data assimilation,  
553 *Mon. Wea. Rev.*, *134*(10), 2888-2899

554 Wang, B., and Y. Zhao (2005), A new data assimilation approach, *Acta Meteorol Sin*, 63, 694-  
555 700. (in Chinese)

556 Xu, Q. (1996), Generalized adjoint for physical processes with parameterized discontinuities.  
557 Part I: basis issues and heuristic examples, *J Atmos Sci*, 53(8),1123-1142.

558 Uzunoglu, B., S. J. Fletcher, M. Zupanski, and I. M. Navon (2007), Adaptive ensemble reduction  
559 and inflation, *Quarterly Journal of the Royal Meteorological Society*, 133(626),1281-1294,  
560 Part A.

561 Volkwein, S. (2008), Model Reduction using Proper Orthogonal Decomposition., Script in  
562 English language, 41 pages, available as a PDF-file. Available from: [http://www.uni-](http://www.uni-graz.at/imawww/volkwein/publist.html)  
563 [graz.at/imawww/volkwein/publist.html](http://www.uni-graz.at/imawww/volkwein/publist.html)

564 Zhang, S.L. Z. Xie, and X. Tian et al.(2006), A soil moisture assimilation scheme with an  
565 unsaturated soil water flow model and in-site observation, *Advances in earth science*,  
566 12,1350-1362, (in Chinese).

567 Zupanski, M. (2005), Maximum likelihood ensemble filter: theoretical aspects, *Mon. Wea.*  
568 *Rev.*,133,1710–1726.

569 FIGURE CAPTIONS:

570 **FIG. 1.** The “perfect” (solid line) and “imperfect” (dashed line) infiltration time series used in the  
571 assimilation experiments.

572 **FIG. 2.** The “perfect” (solid line) and “imperfect” (dashed line) initial soil moisture profiles used  
573 in the assimilation experiments.

574 **FIG. 3.** Relative error ( $E_n$ ) for analyzed soil moisture in the assimilation experiments by the  
575 perfect model with the “imperfect” initial field.

576 **FIG. 4.** Relative error ( $E_n$ ) for analyzed soil moisture in the assimilation experiments by the  
577 imperfect model with the “imperfect” initial field.

579

580

581

582

583

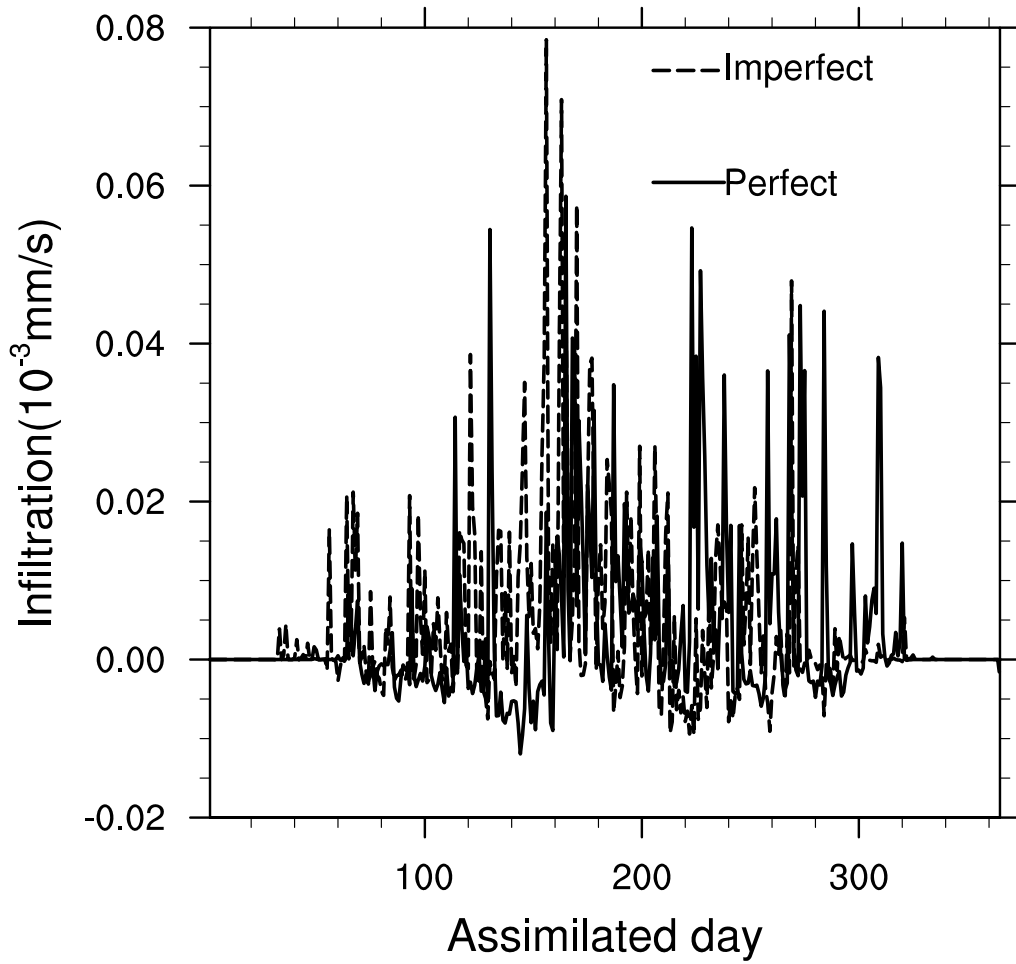
584

585

586

587

588



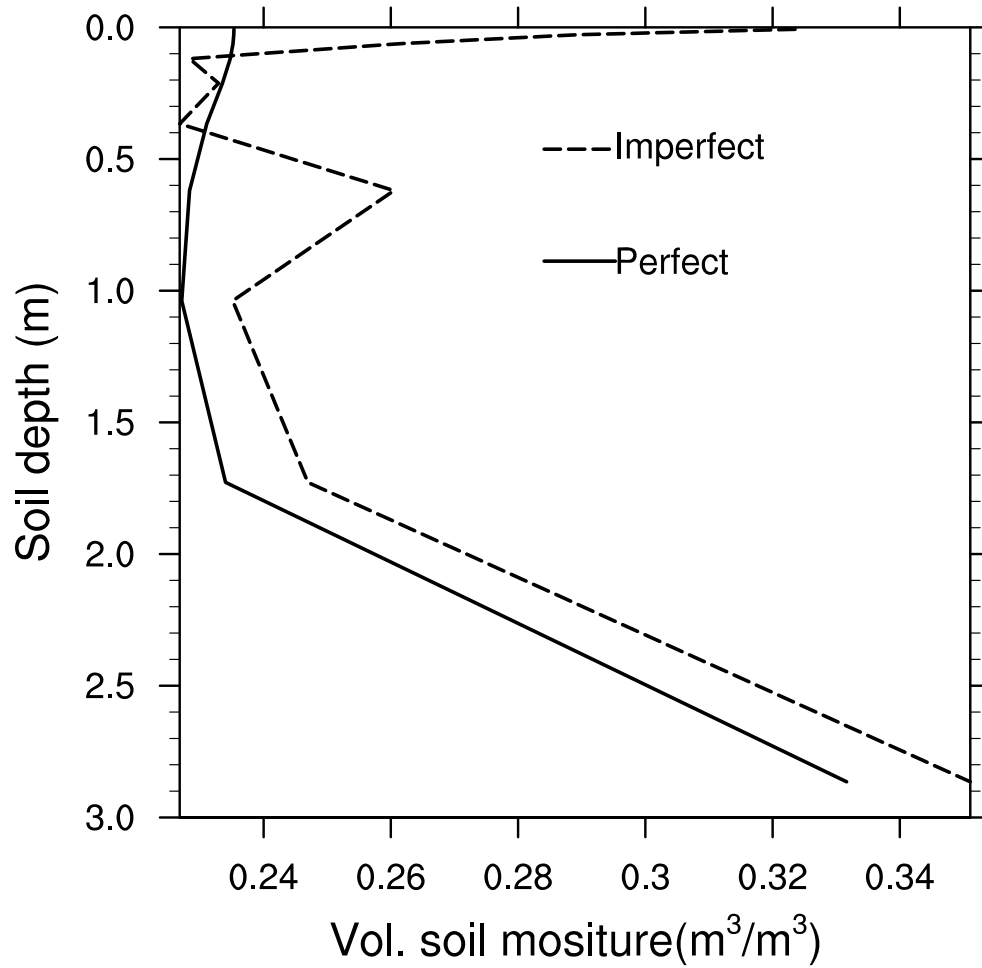
589

590 **FIG.1.** The “perfect” (solid line) and “imperfect” (dashed line) infiltration time series used in the  
 591 assimilation experiments.

592

593

594



595

596 **FIG.2.** The “perfect” (solid line) and “imperfect” (dashed line) initial soil moisture profiles used  
 597 in the assimilation experiments.

598

599

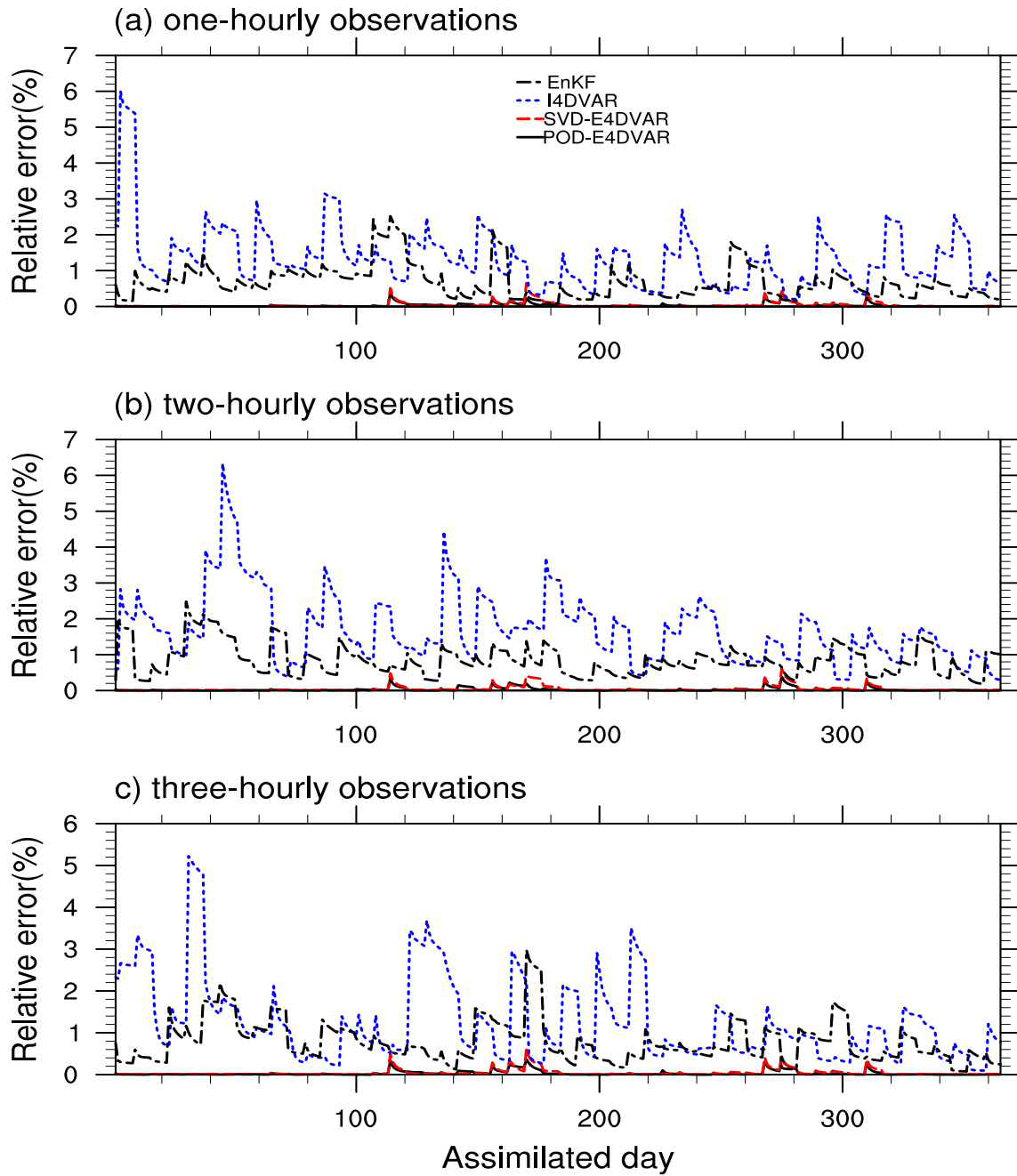
600

601

602

603

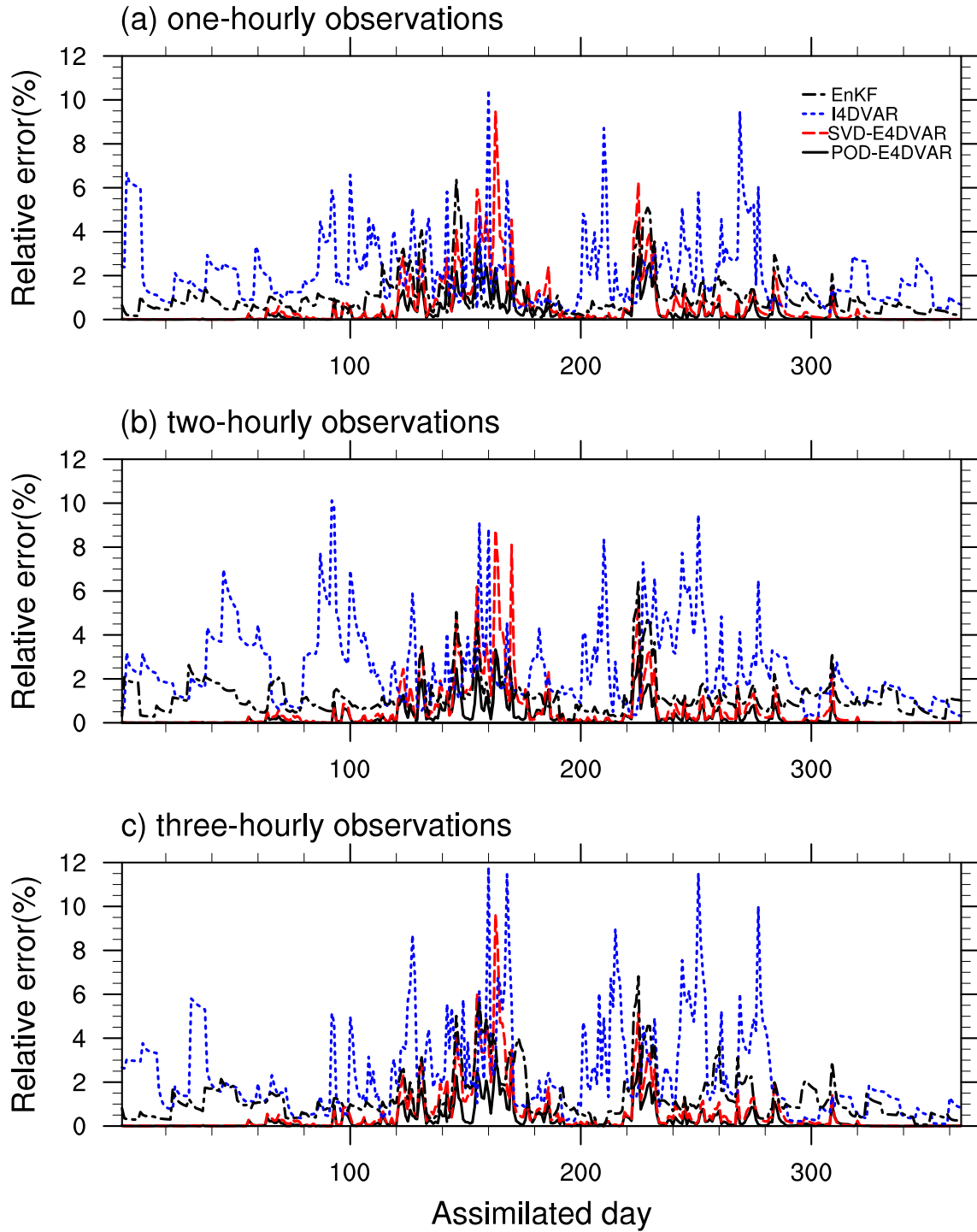
604



606

607 **FIG.3.** Relative error ( $E_n$ ) for analyzed soil moisture in the assimilation experiments by the

608 perfect model with the “imperfect” initial field.



609

610 **FIG.4.** Relative error ( $E_n$ ) for analyzed soil moisture in the assimilation experiments by the  
 611 imperfect model with the “imperfect” initial field.